HHS Public Access

Author manuscript

*Free Radic Biol Med*. Author manuscript; available in PMC 2016 June 28.

Published in final edited form as:

*Free Radic Biol Med*. 2015 December ; 89: 20–33. doi:10.1016/j.freeradbiomed.2015.07.007.

# Whole transcriptome analysis reveals a role for OGG1-initiated DNA repair signaling in airway remodeling

**Leopoldo Aguilera-Aguirre**[a], **Koa Hosoki**[b], **Attila Bacsi**[a,1], **Zsolt Radák**[a,2], **Sanjiv Sur**[b,c], **Muralidhar L. Hegde**[d,3], **Bing Tian**[b,c], **Alfredo Saavedra-Molina**[a,4], **Allan R. Brasier**[b,c], **Xueqing Ba**[a,5], and **Istvan Boldogh**[a,c,*]

[a]Department of Microbiology and Immunology, University of Texas Medical Branch, Galveston, TX 77555, USA

[b]Department of Internal Medicine, University of Texas Medical Branch, Galveston, TX 77555, USA

[c]Sealy Center for Molecular Medicine, and, University of Texas Medical Branch, Galveston, TX 77555, USA

[d]Department of Biochemistry and Molecular Biology, University of Texas Medical Branch, Galveston, TX 77555, USA

## Abstract

Reactive oxygen species (ROS) generated by environmental exposures, and endogenously as by-products of respiration, oxidatively modify biomolecules including DNA. Accumulation of ROS-induced DNA damage has been implicated in various diseases that involve inflammatory processes, and efficient DNA repair is considered critical in preventing such diseases. One of the most abundant DNA base lesions is 7,8-dihydro-8-oxoguanine (8-oxoG), which is repaired by the 8-oxoguanine DNA glycosylase 1 (OGG1)-initiated base-excision repair (OGG1-BER) pathway. Recent studies have shown that the OGG1-BER byproduct 8-oxoG base forms a complex with cytosolic OGG1, activating small GTPases and downstream cell signaling in cultured cells and lungs. This implies that persistent OGG1-BER could result in signaling leading to histological changes in airways. To test this, we mimicked OGG1-BER by repeatedly challenging airways with its repair product 8-oxoG base. Gene expression was analyzed by RNA sequencing (RNA-Seq) and qRT-PCR, and datasets were evaluated by gene ontology and statistical tools. RNA-Seq analysis identified 3252 differentially expressed transcripts (2435 up- and 817 downregulated, Z3-fold change). Among the upregulated transcripts, 2080 mRNAs were identified whose encoded protein products were involved in modulation of the actin family cytoskeleton, extracellular matrix, cell adhesion, cadherin, and cell junctions, affecting biological processes such as tissue

[*]Corresponding author at: Sealy Center for Molecular Medicine, and, University of Texas Medical Branch, Galveston, TX 77555, USA. Fax: +409 747 6869. sboldogh@utmb.edu (I. Boldogh).

[1]Current address: Institute of Immunology, Medical and Health Science Center, University of Debrecen, Debrecen H-4012, Hungary

[2]Current address: Research Institute of Sport Science, Semmelweis University, Budapest H-1025, Hungary

[3]Current address: Radiation Oncology and Neurology, Methodist Research Institute, Houston, TX 77030, USA

[4]Current address: Instituto de Investigaciones Químico-Biológicas, Universidad Michoacana de San Nicolás de Hidalgo, Morelia, Michoacan 58030, Mexico

[5]Current address: Key Laboratory of Molecular Epigenetics, Institute of Genetics and Cytology, Northeast Normal University, Changchun 130024, China

development, cell-to-cell adhesion, cell communication, and the immune system. These data are supported by histological observations showing epithelial alterations, subepithelial fibrosis, and collagen deposits in the lungs. These data imply that continuous challenge by the environment and consequent OGG1-BER-driven signaling trigger gene expression consistent with airway remodeling.

**Keywords**

OGG1-BER; 8-Oxoguanine; Airway remodeling

Airway remodeling is characterized by subepithelial fibrosis, myofibroblast hyperplasia, thickening of the lamina reticularis, and collagen deposition. These histological changes, a decline in lung function, and a poor response to various therapies are common in chronic lung diseases such as asthma and COPD [1, 2]. The underlying molecular mechanisms of tissue remodeling are not fully understood, but in most cases, they are linked to chronic inflammation continuously generating mediators and reactive oxygen species (ROS), which are also considered signaling entities and indiscriminately cause damage to various biomolecules, including DNA [3]. The primary target of ROS in the DNA is guanine, because of its lowest oxidation potential among the DNA bases [4, 5]. Among guanine's oxidation products, 7,8-dihydro-8-oxoguanine (8-oxoG) is the most abundant in both DNA and RNA, and its accumulation in DNA is considered one of the best biomarkers of oxidative stress [6, 7]. 8-OxoG does not induce changes in DNA structure and is not an obstacle to DNA or RNA polymerases [8, 9]. However, 8-oxoG is capable of pairing with adenine in its "*syn*" conformation and is considered one of the most mutagenic base lesions [10]. 8-OxoG must thus be removed to maintain genomic integrity; this occurs primarily via the 8-oxoguanine DNA glycosylase 1 (OGG1)-initiated DNA base-excision repair (OGG1-BER) pathway [11, 12].

Our recent studies documented the association of OGG1-BER with activation of rat viral sarcoma oncogene homolog (Ras) family small GTPases [13]. The pathway's repair product, free 8-oxoG base, forms a complex with cytosolic OGG1. The resulting conformational change allows its interaction with small GTPases, including Kirstein (K)-Ras, which activates them [13–16]. The end result includes the activation of v-Raf-leukemia viral oncogene 1 and phosphatidylinositol, mitogen, stress-activated, and IκB kinases as well as nuclear factor-KB, resulting in robust innate inflammation in the mouse airways [14, 17]. Additional studies showed that OGG1-BER activates Rac1 GTPase, which is involved in cell redox balance [15], and RhoA GTPase, which induces ocsmooth muscle actin polymerization into stress fibers [16]. Studies have also shown that after administration of a high-fat diet, *Ogg1*$^{-/-}$ mice have increased plasma insulin levels, impaired glucose tolerance, enhanced adiposity, and increased hepatic steatosis compared to similarly fed wild-type animals [18]. Another study documented an essential role for OGG1 in embryonic development, because its absence resulted in abnormalities such as severe brain defects [19]. It has recently been shown that OGG1-BER mimicked by a single 8-oxoG challenge increased gene expression involved in homeostatic, immune system, and macrophage

activation processes mediated by chemokines, cytokines, integrin, and interleukin signaling pathways [20].

In the present study, we postulated that continuous repair of oxidatively damaged DNA by OGG1-BER and consequent downstream signaling via small GTPases, induces gene expression, which results in functional and structural changes in lungs. To test this hypothesis, we repeatedly challenged mouse lungs with 8-oxoG to mimic ongoing OGG1-BER after environmental exposures and/or during chronic inflammation. RNA was isolated and analyzed by RNA-Seq. Gene ontology analysis showed that the OGG1-BER product 8-oxoG induced gene expression and signaling pathways consistent with histological changes, including epithelial alterations, increased smooth muscle mass, and collagen deposits in the airways.

## 1. Materials and methods

### 1.1. Animals and treatment

Animal experiments were performed according to the NIH *Guide for Care and Use of Experimental Animals* and approved by the University of Texas Medical Branch (UTMB) Animal Care and Use Committee (Approval No. 0807044A). Eight-week-old female BALB/c mice (The Jackson Laboratory, Bar Harbor, ME, USA) were used for these studies. Mice ($n = 5$ per group) were challenged intranasally (i.n.) on day 0 (single challenge) or days 0, 2, and 4 (multiple challenge) with 60 μl of pH-balanced 8-oxoG (Cayman Chemicals, Ann Arbor, MI, USA) solution (pH 7.4; 0.0005 mg/kg) or saline under mild anesthesia [13]. In controls, we used identical concentrations of 7,8-dihydro-8-oxoadenine (BioLog Life Science Institute, Axxora, San Diego, CA, USA), 8-oxodeoxyguanosine (Sigma–Aldrich (St. Louis, MO, USA), and guanine (Sigma–Aldrich. The lipopolysaccharide concentration was below detectable levels in all reagents. Animals were sacrificed at various time points (0, 30, 60, and 120 min) after the single or multiple challenges to isolate lung RNA.

### 1.2. RNA isolation

After intranasal challenge, mouse lungs were excised and homogenized in lysis buffer (Qiagen, Valencia, CA, USA) with a TissueMiser (Fisher, Pittsburgh, PA, USA). RNA was extracted using an RNeasy kit (Qiagen) per the manufacturer's instructions. Briefly, lung tissue homogenate was loaded onto an RNeasy column and subjected to washes with RW1 and RPE buffers. RNA was eluted with the RNase-free water included in the kit. Eluted RNA was digested with RNase-free DNase as previously described [21]. The RNA concentration was determined spectrophotometrically on an Epoch Take-3 system (Biotek, Winooski, VT, USA) using Gen5 version 2.01 software. Equal amounts of RNA from each mouse lung within an experimental group ($n = 5$) were pooled and analyzed in triplicate. The quality of the total RNA was confirmed spectrophotometrically via the 260/280 nm ratio, which varied from 1.9 to 2.0. RNA integrity was also evaluated by agarose gel electrophoresis.

### 1.3. Next-generation RNA sequencing

Library construction and deep sequencing analysis were performed in UTMB's Next-Generation Sequencing Core Facility (Dr. Thomas G. Wood, Director) on an Illumina HiSeq 1000 sequencing system (Illumina, San Diego, CA, USA). Poly(A)$^+$ RNA was selected from total RNA (1 μg) with poly(T) oligo-attached magnetic beads. Bound RNA was fragmented by incubation at 94 °C for 8 min in 19.5 μl of fragmentation buffer (Illumina, Part 15016648). First-and second-strand synthesis, adapter ligation, and amplification of the library were performed using the Illumina TruSeq RNA sample preparation kit per the manufacturer's instructions. Samples were tracked through the "index tags" incorporated into the adapters. Library quality was evaluated using an Agilent DNA-1000 chip on an Agilent 2100 bioanalyzer. Library DNA templates were quantitated by qPCR and a known-size reference standard.

Cluster formation of the library DNA templates was performed using the TruSeq PE Cluster Kit version 3 (Illumina) and the Illumina cBot workstation under the conditions recommended by the manufacturer. Template input was adjusted to obtain a cluster density of 700–1000 K/mm$^2$. Paired-end, 50-base sequencing-by-synthesis was performed with a TruSeq SBS Kit version 3 (Illumina) on an Illumina HiSeq 1000 per the manufacturer's protocols. Base calls were converted to sequence reads using CASAVA-1.8.2. Sequence data were analyzed with the Bowtie2, Tophat, and Cufflinks programs using the National Center for Biotechnology Information's (NCBI's) mouse (*Mus musculus*) genome build reference mm10. RNA-Seq data have been deposited in the NCBI's Gene Expression Omnibus (GEO) and are accessible through GEO Series Accession No. GSE65031. Reads per kilobase of transcript per million (RPKM) were normalized to the corresponding control for each experimental group [22].

### 1.4. Gene ontology analysis

Heat maps and hierarchical clusters from whole transcriptomes were constructed with GENE-E online software (version 3.0.204) from the Broad Institute (http://www.broadinstitute.org/cancer/software/GENE-E/). Venn diagrams were constructed using online Venny software (version 2.0.2) (http://bioinfogp.cnb.csic.es/tools/venny/). Gene ontologies (GOs) and signaling pathways were analyzed by the PANTHER (Protein Analysis through Evolutionary Relationships, version 9.0) classification system (http://www.pantherdb.org/). The lists of differentially expressed genes (fold change ≥ 3) were processed via GO annotations in this database (22,160 genes, for *M. musculus*). PANTHER's overrepresentation test uses the binomial method with Bonferroni correction for multiple comparisons to annotate classification categories for a list of genes [23, 24]. $P$ values <0.05 were considered significant. The overrepresentation test was used to identify functional classes from the submitted gene lists according to PANTHER's reference lists. This test assumes that under the null hypothesis, genes in the uploaded list are sampled from the same general population as genes from the reference set, i.e., the probability $P$(C) of observing a gene from a particular category C in the uploaded list is the same as in the database reference list [24].

To analyze multiple time points (0, 30, 60, 120 min) Gene Set Enrichment Analysis (GSEA version 2.0.14, Broad Institute; http://www.broad.mit.edu/gsea) was undertaken. The gene sets used were from the Molecular Signatures Database (MsigDB), catalog C5 (version 5.0) functional sets [25].

### 1.5. qRT-PCR

Total RNA (1 μg) was reverse-transcribed using the SuperScript III First-Strand Synthesis System (Invitrogen) per the manufacturer's instructions. To confirm transcript levels for selected genes, an SAB Biosciences RT Profiler PCR Array assay (PAMM-090A, Qiagen) was used per the manufacturer's instructions, using SYBR green. qRT-PCR was performed on an ABI7000 sequence detector (Life Technologies, Grand Island, NY, USA). The amplification thermal profile was 2 min at 50 °C, 10 min at 95 °C, and 1 s at 95 °C followed by 1 min at 60 °C (40 cycles). To confirm the presence of a single product after amplification, a dissociation stage was carried out: 15 s at 95 °C, 20 s at 60 °C, and 15 s at 95 °C. Quantification of changes in gene expression was calculated by using the **ΔΔ**Ct method and unstimulated cells as the calibrator and then normalized to glyceraldehyde-3-phosphate dehydrogenase [26].

### 1.6. Lung histology

After repeated nasal challenges with 8-oxoG (or phosphate-buffered saline (PBS) as a control), mice were sacrificed on day 22. After bronchoalveolar lavage, the lungs were fixed with 10% paraformaldehyde, embedded in paraffin, sectioned at 5 μm, and stained with hematoxylin and eosin and Masson's trichrome by UTMB's Research Histopathology Core. The stained lung sections were analyzed and representative fields photographed using an Olympus BX53F microscope system coupled to an Olympus microscope digital camera DP73 controlled by cellSens Dimension version 1.7 software (Olympus Corp.).

### 1.7. Statistical analysis

Statistical analysis was performed using Student's t test or ANOVA, followed by post hoc tests: Bonferroni's and Dunnett's T3 with SPSS 14.0 software. The data are presented as the means±the standard error of the mean. Differences were considered statistically significant at $p<0.05$.

## 2. Results

### 2.1. Whole transcriptome changes induced by 8-oxoG challenge

Mouse lungs were challenged i.n. with 8-oxoG base on days 0, 2, and 4 and were harvested at 0, 30, 60, and 120 min after the last challenge. Total RNA was isolated and subjected to RNA-Seq analysis. A total of 18,678 transcripts were identified (GEO Series Accession No. GSE65031). Transcript levels (represented by RPKM) at 30, 60, and 120 min were normalized to the corresponding RPKM level at 0 min to calculate fold changes. To visualize the expression patterns at every time point, we generated a heat map using GENE-E online software (Broad Institute). Unsupervised hierarchical clustering of our whole-genome data resulted in two major clusters of transcripts (Fig. 1A). In general, cluster 1 contained 8273 transcripts that were mostly downregulated. Cluster 2 contained 10,414

transcripts, most of which showed increased expression levels. Red tones represent expression values greater than onefold, and green tones show expression less than onefold.

The number of significantly upregulated (≥3-fold) or down-regulated (≤3-fold) transcripts (mRNAs, noncoding transcripts, and miRNAs) in each cluster at every time point is depicted in Fig. 1B. Venn diagrams show the unique and overlapping, differentially expressed transcripts at each time point after 8-oxoG challenge (Fig. 1C) corresponding to the transcripts described in Fig. 1B. Whole transcriptome data showed significant upregulation of 1623 common transcripts and 256, 373, and 259 unique transcripts at 30, 60, and 120 min, respectively. In addition to the unique and common transcripts at all time points, 581 upregulated transcripts were shared between any two time points (Fig. 1C, top). The total of significantly upregulated transcripts at any time point was 3092, of which 2435 were seen at 60 min. Among the 1012 downregulated transcripts at any time point, 59 were common, whereas 99, 571, and 71 were unique at 30, 60, and 120 min, respectively. A total of 212 transcripts were shared only between any two time points (Fig. 1C, bottom).

Kinetically, there was a robust increase in upregulation of transcripts within the first 30 min; they remained nearly steady until 60 min and then started decreasing (Fig. 1D, top). On the other hand, the number of downregulated transcripts peaked at 60 min and substantially decreased at 120 min (Fig. 1D, bottom).

### 2.2. Overrepresentation of gene ontology categories

We performed GO analyses using the PANTHER classification system to determine overrepresented biological processes associated with OGG1-BER-induced gene expression. As described above, the peak in the number of differentially expressed transcripts was reached at 60 min and decreased at later time points. Thus we chose the 60-min time point for GO analysis. Briefly, the list containing 2435 transcripts was submitted to PANTHER analysis, which identified 2080 mRNAs distributed across various GO categories. The remaining 355 transcripts included 39 miRNAs and 316 full-length, noncoding RNAs, whose roles will be analyzed in future studies.

The highest overrepresented biological processes (Fig. 2A) were developmental processes ($P=3.80 \times 10^{-33}$), system development ($P=7.60 \times 10^{-33}$), cellular processes ($P=4.57 \times 10^{-31}$), cell adhesion ($P=7.16 \times 10^{-28}$), biological adhesion ($P=7.16 \times 10^{-28}$), cell communication ($P=9.91 \times 10^{-28}$), immune system processes ($P= 9.37 \times 10^{-24}$), and cell-to-cell adhesion ($P=1.05 \times 10^{-22}$), among others. Several of the most overrepresented protein classes (Fig. 2B) were related to tissue morphology and remodeling, for example, extracellular matrix (ECM) protein ($P=2.64\times 10^{-23}$), cell adhesion molecules ($P=1.57 \times 10^{-15}$), structural proteins ($P=6.94 \times 10^{-8}$), actin family cytoskeletal proteins ($P=4.32 \times 10^{-6}$), ECM structural proteins ($P=8.27 \times 10^{-6}$), cadherins ($P=1.47 \times 10^{-5}$), protease inhibitors ($P=6.79 \times 10^{-5}$), metalloproteinases ($P=2.03 \times 10^{-4}$), cytoskeletal proteins ($P=5.59 \times 10^{-4}$), serine protease inhibitors ($P=7.39 \times 10^{-4}$), cell junction proteins ($P=2.29 \times 10^{-3}$), intermediate filaments ($P=2.51 \times 10^{-3}$), and ECM glycoproteins ($P=3.20 \times 10^{-3}$). Other overrepresented protein classes were related to the immune system, such as the defense/immunity protein ($P=3.69 \times 10^{-10}$) and immunoglobulin receptor superfamily ($P=3.20 \times 10^{-2}$). The most overrepresented cellular components (Fig. 2C) were extracellular

region ($P$=7.33 × $10^{-27}$), ECM ($P$=5.49 × $10^{-19}$), cell part ($P$= 1.14 × $10^{-7}$), intracellular ($P$=3.84 × $10^{-5}$), membrane ($P$=1.49 × $10^{-4}$), plasma membrane ($P$=8.20× $10^{-4}$), and intermediate filament cytoskeleton ($P$=3.84 × $10^{-3}$). The overrepresented molecular functions included various processes involved in tissue remodeling and immune responses. For example, protein binding ($P$=2.74 × $10^{-9}$), structural molecule activity ($P$=3.37 × $10^{-7}$), ECM structural constituents ($P$=1.62 × $10^{-5}$), peptidase inhibitor activity ($P$=5.96× $10^{-5}$), metallopeptidase activity ($P$=1.78 × $10^{-4}$), and peptidase activity ($P$=3.47 × $10^{-4}$), among others (Fig. 2D), are related to tissue remodeling.

The overrepresentation tests undertaken by the PANTHER system were further validated using statistical functional enrichment analysis, which reflects the degree to which a gene set is overrepresented at the top or bottom of a ranked list of genes associated with biological processes [25]. For this purpose, we utilized GSEA (Materials and methods), which considers the positive and negative ranked list matrix to define enrichment scores (ES) of gene sets. The ES is the maximum deviation from zero; thus a positive ES indicates gene set enrichment at the top of the ranked list (red); negative ES indicates gene set enrichment at the bottom of the list (blue) (Figs. 2A and 2B, insets; Fig. 2C, right; and Fig. 2D, bottom). The selected gene ontology categories identified by PANTHER are in line with those generated by GSEA, including biological process (e.g., development, ES=0.382; Fig. 2A, inset), protein class (e.g., extracellular matrix, ES=0.474; Fig. 2B, inset), cellular component (e.g., extracellular component including membrane, plasma membrane, ES=0.483; Fig. 2C, right), and molecular function (e.g., transporter, ES=0.0384, Fig. 2D, bottom). Other GSEA statistical parameters ($q$ and $p$ values) are included in the respective figures.

### 2.3. OGG1-BER-induced signaling pathways

Next, we analyzed signaling pathways by submitting the list of 2080 upregulated mRNAs (≥ 3-fold, at 60 min) to the PANTHER database. The analysis revealed overrepresentation of cadherin, integrin, Rho GTPase, TGF-$\beta$, Wnt, and cytokine/chemokine signaling pathways (Fig. 3, Table 1).

**2.3.1. Cadherin signaling pathway—**OGG1-BER induced the expression of 37 (28.8%) of a total of 128 genes from this pathway with an overrepresentation $P$ value of 7.61 × $10^{-7}$. The cadherin signaling pathway is involved in many biological processes, such as development, cell adhesion, and inflammation. In general, cadherins are transmembrane proteins that play important roles in cell adhesion, forming adherens junctions [27]. The cadherin genes *Cdh2, Cdh3, Cdh6, Cdh8, Cdh13, Cdh15*, and *Cdh19* showed increased expression. On the other hand, the protocadherin genes *Pcdh7, Pcdh9, Pcdh15, Pcdh20, Pcdhb2, Pcdhb4, Pcdhb8, Pcdhb10*, *Pcdhb11, Pcdhb12, Pcdhb13*, and *Pcdhb21* were also upregulated. Their protein products mediate cell-to-cell adhesion and are involved in development and tissue morphogenesis [28]. The catenin family genes *Ctnna2* and *Ctnna3* showed increased expression levels. Catenins contribute to the indirect association of cadherins with the underlying actin cytoskeleton and also function at desmosomes. In addition, they modulate cadherin endocytosis and small GTPases [29]. Actin 1$\alpha$ (*Acta1*), a typical skeletal muscle protein that can induce the expression of various myogenic genes, and actin, $\alpha$, cardiac muscle 1 (*Actc1*) were also upregulated. The epidermal growth factor

receptor (*Egfr*) gene encodes a receptor that binds both EGF and transforming growth factor α (TGF-α), which are involved in cell migration, adhesion, and proliferation. Other upregulated genes involved in the cadherin signaling pathway were v-erb-b2 erythroblastic leukemia viral oncogene homologs 3 (Erbb3) and 4 (Erbb4), which are expressed in skin, lungs, and intestinal epithelium, to induce a variety of cellular responses, including mitogenesis and differentiation. The atypical cadherin family member Fat3 regulates cell polarity [30], and the frizzled protein genes *Fzd4, Fzd9*, and *Fzd10* are involved in regulating the cytoskeleton. Additionally, lymphoid enhancer binding factor 1 (*Lef1*) also showed increased levels. The product of Lef1 is a transcription factor that decreases the expression of *Cdh1* and is highly expressed in lung cancers [31]. Other upregulated genes included the wingless-type mouse mammary virus tumor integration site family (*Wnt4, Wnt5a, Wnt10a, Wnt2b, Wnt7b*, and *Wnt9b*), whose products are involved in regulation of the cytoskeleton.

**2.3.2. Integrin signaling pathway—**This pathway showed increased expression of 42 (24.0%) of 175 genes and an overrepresentation value of $P = 6.68 \times 10^{-6}$. Integrins are transmembrane receptors that interact with the ECM to form bridges between cells; they can also transduce signals from the exterior of the cell to sense the composition and mechanical features of the ECM. Thus, as important components of the ECM, collagens are involved in this relationship and have a role not only as a structural support for connective tissues but also in the integrin signaling pathway [32]. Most of the upregulated genes in this pathway belong to the collagen family (*Col1a1, Col2a1, Col3a1, Col4a1, Col4a2, Col4a3, Col4a4, Col5a1, Col5a2, Col5a3, Col6a3, Col6a6, Col8a1, Col9a1, Col9a2, Col10a1, Col11a1, Col11a2, Col13a1, Col14a1, Col15a1, Col17a1*), followed by the integrin family members integrin α1, α2, and α6 (*Itga1, Itga2, and Itga6*). These integrins can interact with various ligands from the collagen family and laminins in the ECM [33]. Other upregulated integrins were integrin αD (*Itgad*), integrin αM (*Itgam*), and integrin β-like 1 (*Itgbl1*). Laminins are major components of basement membranes and have important roles in lung development and airway remodeling in asthma [34, 35]. Among these, the laminins α-chain 2 and 3 (*Lama2, Lama3*) were upregulated. Laminin β1 (*Lamb1*) and laminin γ chain 1 (*Lamc1*) expression levels were also increased. Other genes involved in the integrin signaling pathway showing increased expression levels were c-abl oncogene 1, non-receptor tyrosine kinase (*Abl1*); ADP-ribosylation factor-like 1 (*Arl1*); ArfGAP with SH3 domain, ankyrin repeat, and PH domain1 (*Asap1*); v-crk sarcoma virus CT10 oncogene homolog (avian)-like (*Crkl*); mitogen-activated protein kinase 6 (*Mapk6*); multiple EGF-like-domains 9 (*Megf9*); netrin 4 (*Ntn4*); and phosphatidylinositol 3-kinase, regulatory subunit, polypeptide 1 p85 α (*Pik3r1*).

**2.3.3. Cytoskeletal regulation by Rho GTPases—**The number of upregulated genes related to this pathway was 19 (23.75%) of a total of 80. The overrepresentation test gave a $P = 4.96 \times 10^{-2}$. Rho GTPases regulate the cytoskeleton by increasing the amount of stress fibers and focal adhesions that mediate the cell responses to ECM adhesion. Upregulated genes related to this pathway were the myosin heavy chain family members 1–4, 10, 11, and 13 (*Myh1, Myh2, Myh3, Myh4, Myh8, Myh9, Myh10, Myh11, Myh13*) and myosin light chain kinase 2 (*Mylk2*). The diaphanous homologs 1 and 3 (*Diap1, Diap3*)-

encoded proteins are downstream targets of Rho involved in the activation of proto-oncogene tyrosine-protein kinase Src [36] and filopodia formation [37]. Other upregulated genes were *Acta1, Actc1, Pak3, Ssh1*, and *Tubb1.*

**2.3.4. Wnt signaling pathway—**Fifty-seven (20.9%) of 272 genes in this pathway showed increased expression, with an overrepresentation value of $P=6.68 \times 10^{-6}$. The Wnt signaling pathway is involved in a variety of cellular processes including cell fate determination, cell migration, cell polarity, and organogenesis during embryonic development and is involved in pathological processes such as carcinogenesis [36], cardiac hypertrophy/remodeling [38], pulmonary fibrosis [39], and airway remodeling [40]. Upregulated genes in the Wnt signaling pathways were cadherins (*Cdh2, Cdh3, Cdh6, Cdh8, Cdh13, Cdh15, Cdh19*), protocadherins (*Pcdh7, Pcdh9, Pcdh15, Pcdh20, Pcdhb2, Pcdhb4, Pcdhb8, Pcdhb10, Pcdhb11, Pcdhb12, Pcdhb13, Pcdhb21*), Wnt family members (*Wnt10a, Wnt2b, Wnt4, Wnt5a, Wnt7b, Wnt9b*), and frizzled (FZD)-related genes (*Frzb, Fzd4, Fzd9, Fzd10*), whose products are the ligands for the FZD family of receptors (regulating cytoskeleton, cell shape, cell proliferation, and cell migration). In addition, genes encoding secreted frizzled-related proteins (*Sfrp1, Sfrp2*, and *Sfrp4*) and myosin heavy polypeptides (*Myh1, Myh2, Myh3, Myh4, Myh8, Myh13*), as well as *Tnf Edn1, Fat3, Gng3, Itpr2, Lef1, Lrp5, Nfatc2, Nkd2, Plcb4, Tbl1x*, and *Tcf7*, were upregulated.

**2.3.5. Transforming growth factor β signaling pathway—**In this pathway, 17 (17.9%) of 97 genes showed increased expression. These included transforming growth factor $\beta 2$ (*Tgfb2*, which encodes a major profibrotic cytokine and is involved in a wide range of functions, including angiogenesis and changes in ECM [41]); tolloid-like transcript (*Tll1*, encodes a metalloprotease); FYVE domain-containing 9 (*Zfyve9*, whose protein product is involved in the regulation of TGF-$\beta$ signaling by interacting with SMAD2 and SMAD3 [42]); *Bmp5, Bmp6*, and *Bmp8a* (which encode bone morphogenetic proteins); the bone morphogenetic protein receptor type II (*Bmpr2*, which is a serine/threonine kinase); *Gdf2, Gdf6*, and *Gdf11* (growth differentiation factors); and activin A receptors (*Acvr1b, Acvr1c*). Importantly, there were upregulated transcription-related genes, encoding CBP/p300-interacting transactivator with a Glu/Asp-rich carboxy-terminal domain 4 (*Cited4*), cAMP-response element-binding protein (*Crebbp*, a transcription cofactor), the transcription factors Fos-like antigen 1 (*Fosl1*) and forkhead box H1 (*Foxh1*), and myostatin (*Mstn*, which inhibits muscle differentiation and growth [43]).

**2.3.6. Chemokine and cytokine signaling pathway—**The number of upregulated genes in this pathway was 43 (18.4%) of 234 and the overrepresentation P value was $6.56 \times 10^{-3}$. Among the genes having significantly increased expression levels were six C-C motif chemokines (*Ccl3, Ccr4, Ccr6, Ccr8, Ccr9*, and *Ccl20*); eight C-X-C motif chemokines (*Cxcl1, Cxcl2, Cxcl3, Cxcl9, Cxcl10, Cxcl11, Cxcl12*, and *Cxcl13*); interleukins 1$\alpha$, 10, and 17C (*IL1a, IL10, IL17c*) and the interleukin 2 receptor, $\beta$ chain (*IL2rb*); integrins (*Itga2* and *Itgam*); collagen family members (*Col6a3, Col6a6, Col14a1*); phospholipase Cβ4 (*Plcb4*) and $\gamma 1$ (*Plcg1*); arachidonate 12-lipoxygenase (*Alox12*) and arachidonate lipoxygenase, epidermal (*Alox12e*); adenylate cyclase 5 (*Adcy5*); calcium/calmodulin-dependent protein kinase II$\alpha$ (*Camk2a*); guanine nucleotide-binding protein $\gamma 3$ (*Gng3*); GRB2-related adaptor

protein 2 (*Grap2*); inositol 1,4,5-triphosphate receptor 2 (*Itpr2*); nuclear factor of activated T cells, cytoplasmic, calcineurin-dependent 2 (*Nfatc2*); nuclear factor of κ light polypeptide gene enhancer in B cells inhibitor, α (*Nfkbia*); protein kinase, X-linked (*Prkx*); platelet-activating factor receptor (*Ptafr*); reticuloendotheliosis oncogene (*Rel*); regulator of G-protein signaling 1 (*Rgs1*); suppressor of cytokine signaling 4 (*Socs4*); von Willebrand factor A domain-containing 2 (*Vwa2*); and p21 protein (*Cdc42/Rac*)-activated kinase 3 (*Pak*3). Other signaling pathways with lower levels of representation are shown in Fig. 3.

### 2.4. Validation of RNA-Seq by qRT-PCR

To validate RNA-Seq analysis, we verified the expression levels of selected genes related to airway remodeling by qRT-PCR. To do so we utilized the same RNAs as analyzed by RNA-Seq. Fig. 4 shows a comparison of expression levels or selected genes by RNA-Seq and qRT-PCR. The observed differences in fold changes determined by RNA-Seq and qRT-PCR demonstrated a similar pattern in mRNA levels.

### 2.5. Challenges with 8-oxoG induce tissue remodeling-associated gene expression

The signaling pathways described above reveal that gene expression induced by repeated 8-oxoG challenges resembles that of tissue remodeling (Figs. 2–4), while a single challenge (SC) primarily induced proinflammatory gene expression and inflammation [20]. Therefore additional challenges (Fig. 5A) were applied after inflammatory cells (e.g., neutrophils) were cleared from the lung tissues [20]. Next, we compared the transcript levels derived from time 0 (day 0) to day 4, time 0 (Fig. 5A). The heat maps generated from the RPKM values showed notable differences between SC and multiple challenges (MC, Fig. 5B). Taking the 0 time RPKM values of the SC as onefold (Fig. 5C left panel), we calculated fold change at time 0 from the last challenge of the MC group (day 4) and heat maps were generated to visualize the differences (Fig. 5C, right). These data were further analyzed using the PANTHER database (GO analysis), showing no over-representation of biological processes (data not shown). In contrast, after the normalization of expression levels from time 0 of MC as onefold (Fig. 5D, left), we observed significant changes at 60 min (Fig. 5D, right). These results suggest that the SC with the OGG1-BER product 8-oxoG primarily induced a proinflammatory signaling mediated by cytokine/chemokine and interleukins (ILs) as previously observed [20], while MC activated cadherin, integrin, Rho GTPase, TGF-β, and Wnt signaling pathways (Fig. 3), consistent with tissue remodeling.

### 2.6. Relevance of OGG1-BER-induced gene expression to tissue remodeling in humans

Next, we examined whether multiple 8-oxoG challenge-induced changes in gene expression in mouse lungs resemble those previously associated with human pulmonary remodeling. To address this issue, lists of the human homologs of the mouse genes were created using the PANTHER database. These lists were searched against the GeneCards database (www.genecards.org) containing human genes associated with changes in cytoskeleton, cell adhesion, surfactant, ECM, and cell junctions. As a control, we utilized the RNA-Seq dataset from single challenge (GEO: GSE61095) as previously described [20]. Hierarchically clustered heat maps were generated using GENE-E. The data showed altered/increased expression of genes encoding cytoskeletal, cell adhesion, surfactant, ECM, and cell junction

proteins (Figs. 6A–6F), suggesting that OGG1-BER and downstream signaling could be related to tissue remodeling, not only in the mouse lung model, but also in humans.

### 2.7. Histological changes in the airways after multiple 8-oxoG challenges

To examine the validity of GO analysis showing over-representation of signaling pathways and biological processes (Figs. 2, 3 and Table 1) that could induce histological changes in mouse lungs, airways were challenged as outlined in Fig. 5A. On day 22, lungs were excised, sectioned, and stained with hematoxylin and eosin and Masson's trichrome. Histological examination showed epithelial metaplasia, formation of trophic units, and smooth muscle hyperplasia around the peribronchial area (Fig. 7A). A thickening of the basal membranes was observed as shown in Figs. 7A and 7B (bottom). Fig. 7B (bottom) also shows an excess accumulation of ECM (collagen deposition; blue) in peribronchial areas and formation of fibrous connective tissue (Masson's trichrome staining). In controls, 7,8-dihydro-8-oxoadenine, 2′-deoxyguanosine, guanine (data not shown), or vehicle (PBS) challenge did not cause histological changes. These histological changes are in line with GO analysis showing overrepresentation of tissue remodeling-related biological processes and signaling pathways (Figs. 2, 3, and 6).

## 3. Discussion

8-OxoG is one of the most abundant oxidized base lesions in DNA. It is formed upon environmental oxidant exposure to ROS generated by various cellular oxidoreductases and primarily repaired via the OGG1-BER pathway. It has been shown that the repair product, free 8-oxoG base, forms a complex with cytosolic OGG1 and activates small GTPases [13, 15, 16]. Here we document that mimicking OGG1-BER by repeatedly adding its product 8-oxoG to the airways induced changes in the expression of genes involved in biological processes such as system development, biological adhesion, cell adhesion, cell-to-cell communication, and ECM. These processes were mediated by cadherin-, Wnt-, integrin-, Rho GTPase-, TGF-$\beta$-, chemokine-, cytokine-, and IL-driven signaling pathways and are in line with the observed histological changes in the lungs. Although a great amount of work remains to be done, the present results suggest that continuous repair of 8-oxoG by OGG1-BER results in downstream signaling that may play a role in airway remodeling.

Our previous reports have shown that induction of OGG1-BER in the lungs or exposure of the airways to 8-oxoG, but not to other oxidized DNA bases or guanine, activates Ras family GTPases, leading to downstream signaling and the expression of proinflammatory cytokines and chemokines, resulting in a robust innate immune response [14, 44]. We also documented that activation of Rho-GTPase downstream of OGG1-BER induced smooth muscle α-actin polymerization into stress fibers and increases the level of smooth muscle α-actin in insoluble cellular/tissue fractions [16]. Because small GTPases are central to many (if not all) cell signaling processes, we proposed that by its continuous activation, OGG1-BER is etiologically linked to gene expression responsible for histological structural changes in the airways.

To test this hypothesis, in the present study we repeatedly challenged lungs with the repair product of OGG1-BER, 8-oxoG. This strategy allowed us to avoid inducing oxidative DNA

damage and repair via ROS, which themselves are involved in mediating gene expression and cellular biological processes [45]. Mouse lungs were challenged (dose: 0.0005 μg/g) on days 0, 2, and 4 and lungs were harvested 0, 30, 60, and 120 min after the last challenge. Although RNA-Seq data are available from all time points, detailed analyses were limited to 60 min. The rationale for this experimental design was based on our previous observations showing that de novo-synthesized chemokines/cytokines are present intra- and extracellularly at or after 120 min [14, 44, 46].

Repeated challenge with 8-oxoG base resulted in upregulation of 2080 protein-coding mRNAs, 39 microRNAs, and 326 noncoding, full-length RNAs. Although noncoding RNAs (microRNAs and full-length RNAs) have been recognized as regulatory molecules and are involved in a number of signaling networks and cellular processes [47], here we focused on the biological significance of pathways driven by mRNA-encoded proteins. GO analysis revealed that gene expression was related to various biological processes, of which the most overrepresented were associated with developmental, system developmental, cellular, biological and cell adhesion, intracellular and cell-to-cell communication, and cytoskeletal processes. These processes were primarily driven by cadherin-, Wnt-, integrin-, chemokines-, cytokines-, TGF-$\beta$-, and Rho GTPase-driven signaling pathways. These results are in contrast with our previous studies, in which a single challenge induced processes that were primarily associated with immune homeostasis mediated by cytokines, chemokines, and interleukins [20]. Together, these data and our histological findings support the hypothesis that persistent activation of small GTPase-driven signaling due to continuous genome maintenance by OGG1-BER could be a “root cause” of processes leading to tissue changes in the lungs.

Increased OGG1-BER in the airways and challenging the lungs with 8-oxoG base both induced innate immune responses [14, 44]. Indeed, after each challenge with 8-oxoG we observed recruitment of neutrophils to the lungs, which were cleared within 36 h. Therefore, every challenge was applied every 48 h. Although we rechallenged apparently healthy lungs, an intriguing question remained: were inflammatory mediators or OGG1-BER (8-oxoG challenge) signaling responsible for the observed gene expression favoring biological processes that drive tissue remodeling? In an attempt to answer this complex question, we generated a heat map from transcript levels at time 0 from the last challenge and compared to another heat map generated from transcript levels at time 0 from the start of the experiment. Although we visually observed notable differences among these heat maps, GO analysis showed no overrepresentation of biological processes. In contrast, 60 min later, we unexpectedly observed qualitatively different gene expression and a nearly fivefold increase in the number (2080) of genes compared to that at 60 min (443 genes) from the start of the experiment. The mechanism by which repeated challenges modulate gene expression is being investigated. We undertook studies to examine whether animals are sensitized to 8-oxoG, similar to allergens such as ragweed pollen extract (atopic) [48, 49] or those occurring in response to agents like aspirin (nonatopic) [50]. These studies showed no hyperreactivity-type responses (data not shown). One possibility is that changes in the genome (e.g., chromatin modifications by histone acetylation and/or methylation) allow increased recruitment of regulatory proteins to promoters (e.g., transcription factors, coactivators) [44, 51–55]. At this time, we do not know the mechanism, but if indeed there are genomic

changes after 8-oxoG challenge, OGG1-BER could be a link between oxidant environmental challenges and epigenetic changes in the lungs.

For these studies, we challenged the lungs and isolated RNA from the whole organ, raising the possibility that the fold changes in mRNA levels may actually show transcriptional events not only from the epithelium, representing only 25% of total lung cells [56], but also from the subepithelial regions. At this point, we cannot exclude the contribution of other cell types, e.g., mast or dendritic cells (representing <1% of cells in the lung epithelium). Alveolar resident macrophages are affected by 8-oxoG challenge (unpublished data); however, they were removed before RNA extraction by lavage of the airways. Therefore, we speculate that multiple 8-oxoG challenge-induced changes in gene expression primarily represent the response of the airway epithelium with the possible contribution of subjacent cells. In support of this idea, (a) 8-oxoG is rapidly taken up by cells [57], possibly by the lung epithelium; (b) small GTPases were activated from 15 min on; and (c) robust changes in gene expression were observed from 30 min on (60 min maximum) [20, 46]. The question still remains of how histological changes occur in subepithelial regions. We propose that mediators (e.g., TGF-$\beta$ and growth factors) are synthesized in the epithelial mucosa and released into the surrounding tissues, mediating changes in proliferation and function of underlying cells resulting in increased smooth muscle mass, and ECM levels (Fig. 8). These results are supported by data showing the active participation of airway epithelium in expressing mediators and regulatory molecules responsible for histological changes in lungs [58, 59]. One may also propose that these de novo synthesized mediators induce changes within the epithelium (resulting in their dedifferentiation into pluripotent “stem-like” cells, a process that is part of the epithelial–mesenchymal transition), and then these cells differentiate to, e.g., smooth muscle, which secretes ECM. In support of this possibility, we observed morphological changes in the epithelium, formation of “trophic units,” and submerging of epithelial-like cells to sublayers, which appear to be involved in histological changes.

It has been documented that tissue remodeling is a complex, long-term process requiring chronic or multiple exposures and characterized by subepithelial fibrosis, myofibroblast hyperplasia, thickening of the lamina reticularis, and ECM deposition [1, 2]. In our lung model, multiple (but not single) challenges with 8-oxoG led to gene expression overrepresenting biological processes consistent with histological changes resembling airway remodeling (epithelial dysplasia, subepithelial fibrosis, and excessive ECM). Thus we asked whether OGG1:8-oxoG-driven gene expression in mouse lung has any relevance to tissue remodeling in humans.

To address this question, the human equivalent of the mouse gene list was searched and compared to a list of genes encoding cytoskeletal, cell adhesion, cell junction, surfactant, and ECM proteins. As a control, we utilized the RNA-Seq dataset from a single challenge [20]. We found similarities resulting from multiple (but not single) challenges that are consistent with structural tissue changes in human lungs. Future studies will determine whether OGG1-BER is at least partially related to tissue remodeling in humans.

In summary, based on the results of the current study, we propose that oxidative stress, resulting from repeated environmental oxidant exposures and/or increased activity of cellular oxidoreductases, causes DNA damage and a compensatory increase in OGG1-BER to maintain genomic integrity. Although OGG1's primary function is to prevent mutagenesis, our results suggest that excessive and persistent generation of 8-oxoG and the resulting activation of small GTPases and downstream signaling lead to gene expression changes that are consistent with biological processes shown to be involved in tissue remodeling (a proposed model is shown in Fig. 8). Thus, we raise the possibility that oxidative DNA base damage corrected by OGG1-BER could be a link between multiple environmental exposures and tissue remodeling processes in human airways. Ongoing studies in our laboratory are aimed at further examining the mechanisms of OGG1-BER-driven tissue remodeling, which may provide insights into the rational design of therapeutics.

## Acknowledgments

This work was supported by Grants NIEHSRO1 ES018948 (I.B.) and NIAID/AI062885 (A.R.B., I.B.), NHLBI Proteomic Center Grant N01HV00245 (I.B., S.S.; Dr. A. Kurosky, Director), NIEHS Center Grant P30 ES006676, the International Science–Technology Collaboration Foundation (20120728) of Jilin Province in China (X.B.), the European Union and the European Social Fund, TAMOP 4.2.2.A-11/1/KONV-2012-2023 (A.B.). L. Aguilera-Aguirre is an Environmental Toxicology Research Training Fellow (NIEHS T32 ES007254-22). We thank Mardelle Susman (Department of Microbiology and Immunology) for critically editing the manuscript and Dr. David Konkel (Institute for Translational Sciences, University of Texas Medical Branch) both for his scientific input and for editing the manuscript.

## Abbreviations

| | |
|---|---|
| **8-oxoG** | 7,8-dihydro-8-oxoguanine |
| **BER** | base-excision repair |
| **CASAVA** | consensus assessment of sequence and variation |
| **COPD** | chronic obstructive pulmonary disease |
| **ECM** | extracellular matrix |
| **GENE-E** | a matrix visualization and analysis platform |
| **GEO** | Gene Expression Omnibus |
| **GO** | gene ontology |
| **GSEA** | Gene Set Enrichment Analysis |
| **OGG1** | 8-oxoguanine DNA glycosylase 1 |
| **OGG1-BER** | OGG1-initiated DNA base-excision repair |
| **PANTHER** | protein analysis through evolutionary relationships |
| **RPKM** | reads per kilobase of transcript per million |
| **RNA-Seq** | RNA sequencing |

**ROS** reactive oxygen species

## References


1. Bousquet J, Jeffery PK, Busse WW, Johnson M, Vignola AM. Asthma: from bronchoconstriction to airways inflammation and remodeling. Am J Respir Crit Care Med. 2000; 161:1720–1745. [PubMed: 10806180]
2. James AL, Wenzel S. Clinical relevance of airway remodelling in airway diseases. Eur Respir J. 2007; 30:134–155. [PubMed: 17601971]
3. Cooke MS, Evans MD, Dizdaroglu M, Lunec J. Oxidative DNA damage: mechanisms, mutation, and disease. FASEB J. 2003; 17:1195–1214. [PubMed: 12832285]
4. Steenken S, Jovanovic S. How easily oxidizable is DNA? One-electron reduction potentials of adenosine and guanosine radicals in aqueous solution. J Am Chem Soc. 1997; 119:617–618.
5. Cadet J, Douki T, Gasparutto D, Ravanat JL. Oxidative damage to DNA: formation, measurement and biochemical features. Mutat Res. 2003; 531:5–23. [PubMed: 14637244]
6. Svoboda P, Maekawa M, Kawai K, Tominaga T, Savela K, Kasai H. Urinary 8-hydroxyguanine may be a better marker of oxidative stress than 8-hydro-xydeoxyguanosine in relation to the life spans of various species. Antioxid Redox Signaling. 2006; 8:985–992.
7. Radak Z, Boldogh I. 8-Oxo-7,8-dihydroguanine: links to gene expression, aging, and defense against oxidative stress. Free Radic Biol Med. 2010; 49:587–596. [PubMed: 20483371]
8. Maga G, Villani G, Crespan E, Wimmer U, Ferrari E, Bertocci B, Hubscher U. 8-Oxo-guanine bypass by human DNA polymerases in the presence of auxiliary proteins. Nature. 2007; 447:606–608. [PubMed: 17507928]
9. Larsen E, Kwon K, Coin F, Egly JM, Klungland A. Transcription activities at 8-oxoG lesions in DNA. DNA Repair (Amsterdam). 2004; 3:1457–1468.
10. Damsma GE, Cramer P. Molecular basis of transcriptional mutagenesis at 8-oxoguanine. J Biol Chem. 2009; 284:31658–31663. [PubMed: 19758983]
11. Mitra S, Hazra TK, Roy R, Ikeda S, Biswas T, Lock J, Boldogh I, Izumi T. Complexities of DNA base excision repair in mammalian cells. Mol Cells. 1997; 7:305–312. [PubMed: 9264015]
12. Dizdaroglu M. Substrate specificities and excision kinetics of DNA glycosylases involved in base-excision repair of oxidative DNA damage. Mutat Res. 2003; 531:109–126. [PubMed: 14637249]
13. Boldogh I, Hajas G, Aguilera-Aguirre L, Hegde ML, Radak Z, Bacsi A, Sur S, Hazra TK, Mitra S. Activation of ras signaling pathway by 8-oxoguanine DNA glycosylase bound to its excision product, 8-oxoguanine. J Biol Chem. 2012; 287:20769–20773. [PubMed: 22568941]
14. Aguilera-Aguirre L, Bacsi A, Radak Z, Hazra TK, Mitra S, Sur S, Brasier AR, Ba X, Boldogh I. Innate inflammation induced by the 8-oxoguanine DNA glycosylase-1-KRAS-NF-kappaB pathway. J Immunol. 2014; 193:4643–4653. [PubMed: 25267977]
15. Hajas G, Bacsi A, Aguilera-Aguirre L, Hegde ML, Tapas KH, Sur S, Radak Z, Ba X, Boldogh I. 8-Oxoguanine DNA glycosylase-1 links DNA repair to cellular signaling via the activation of the small GTPase Rac1. Free Radic Biol Med. 2013; 61:384–394. [PubMed: 23612479]
16. Luo J, Hosoki K, Bacsi A, Radak Z, Hegde ML, Sur S, Hazra TK, Brasier AR, Ba X, Boldogh I. 8-Oxoguanine DNA glycosylase-1-mediated DNA repair is associated with Rho GTPase activation and α-smooth muscle actin polymerization. Free Radic Biol Med. 2014; 73:430–438. [PubMed: 24681335]
17. German P, Szaniszlo P, Hajas G, Radak Z, Bacsi A, Hazra TK, Hegde ML, Ba X, Boldogh I. Activation of cellular signaling by 8-oxoguanine DNA gly-cosylase-1-initiated DNA base excision repair. DNA Repair (Amsterdam). 2013; 12:856–863.
18. Sampath H, Vartanian V, Rollins MR, Sakumi K, Nakabeppu Y, Lloyd RS. 8-Oxoguanine DNA glycosylase (OGG1) deficiency increases susceptibility to obesity and metabolic dysfunction. PLoS One. 2012; 7:e51697. 7 2012. [PubMed: 23284747]
19. Gu A, Ji G, Yan L, Zhou Y. The 8-oxoguanine DNA glycosylase 1 (ogg1) decreases the vulnerability of the developing brain to DNA damage. DNA Repair (Amsterdam). 2013; 12:1094–1104.

20. Aguilera-Aguirre L, Hosoki K, Bacsi A, Radak Z, Wood TG, Widen SG, Sur S, Ameredes BT, Saavedra-Molina A, Brasier AR, Ba X, Boldogh I. Whole transcriptome analysis reveals an 8-oxoguanine DNA glycosylase-1-driven DNA repair-dependent gene expression linked to essential biological processes. Free Radic Biol Med. 2015; 81:107–118. [PubMed: 25614460]
21. Aguilera-Aguirre L, Bacsi A, Saavedra-Molina A, Kurosky A, Sur S, Boldogh I. Mitochondrial dysfunction increases allergic airway inflammation. J Immunol. 2009; 183:5379–5387. [PubMed: 19786549]
22. Dillies MA, Rau A, Aubert J, Hennequet-Antier C, Jeanmougin M, Servant N, Keime C, Marot G, Castel D, Estelle J, Guernec G, Jagla B, Jouneau L, Laloe D, Le Gall C, Schaeffer B, Le Crom S, Guedj M, Jaffrezic FA. comprehensive evaluation of normalization methods for Illumina high-throughput RNA sequencing data analysis. Briefings Bioinf. 2013; 14:671–683.
23. Mi H, Thomas P. PANTHER pathway: an ontology-based pathway database coupled with data analysis tools. Methods Mol Biol. 2009; 563:123–140. [PubMed: 19597783]
24. Mi H, Muruganujan A, Casagrande JT, Thomas PD. Large-scale gene function analysis with the PANTHER classification system. Nat Protoc. 2013; 8:1551–1566. [PubMed: 23868073]
25. Subramanian A, Tamayo P, Mootha VK, Mukherjee S, Ebert BL, Gillette MA, Paulovich A, Pomeroy SL, Golub TR, Lander ES, Mesirov JP. Gene set enrichment analysis: a knowledge-based approach for interpreting genome-wide expression profiles. Proc Natl Acad Sci USA. 2005; 102:15545–15550. [PubMed: 16199517]
26. Livak KJ, Schmittgen TD. Analysis of relative gene expression data using realtime quantitative PCR and the 2(−ΔΔC(T)) method. Methods. 2001; 25:402–408. [PubMed: 11846609]
27. van Roy F. Beyond E-cadherin: roles of other cadherin superfamily members in cancer. Nat Rev Cancer. 2014; 14:121–134. [PubMed: 24442140]
28. Halbleib JM, Nelson WJ. Cadherins in development: cell adhesion, sorting, and tissue morphogenesis. Genes Dev. 2006; 20:3199–3214. [PubMed: 17158740]
29. McCrea PD, Gu D. The catenin family at a glance. J Cell Sci. 2010; 123:637–642. [PubMed: 20164302]
30. Katoh Y, Katoh M. Comparative integromics on FAT1, FAT2, FAT3 and FAT4. Int J Mol Med. 2006; 18:523–528. [PubMed: 16865240]
31. Nagathihalli NS, Massion PP, Gonzalez AL, Lu P, Datta PK. Smoking induces epithelial-to-mesenchymal transition in non-small cell lung cancer through HDAC-mediated downregulation of E-cadherin. Mol Cancer Ther. 2012; 11:2362–2372. [PubMed: 22933707]
32. Leitinger B. Transmembrane collagen receptors. Annu Rev Cell Dev Biol. 2011; 27:265–290. [PubMed: 21568710]
33. Thorsteinsdottir S, Deries M, Cachaco AS, Bajanca F. The extracellular matrix dimension of skeletal muscle development. Dev Biol. 2011; 354:191–207. [PubMed: 21420400]
34. Nguyen NM, Senior RM. Laminin isoforms and lung development: all isoforms are not equal. Dev Biol. 2006; 294:271–279. [PubMed: 16643883]
35. Royce SG, Tan L, Koek AA, Tang ML. Effect of extracellular matrix composition on airway epithelial cell and fibroblast structure: implications for airway remodeling in asthma. Ann Allergy Asthma Immunol. 2009; 102:238–246. [PubMed: 19354071]
36. Zhang Y, Morris JP 4th, Yan W, Schofield HK, Gurney A, Simeone DM, Millar SE, Hoey T, Hebrok M, Pasca di Magliano M. Canonical wnt signaling is required for pancreatic carcinogenesis. Cancer Res. 2013; 73:4909–4922. [PubMed: 23761328]
37. Mellor H. The role of formins in filopodia formation. Biochim Biophys Acta. 2010; 1803:191–200. [PubMed: 19171166]
38. Malekar P, Hagenmueller M, Anyanwu A, Buss S, Streit MR, Weiss CS, Wolf D, Riffel J, Bauer A, Katus HA, Hardt SE. Wnt signaling is critical for maladaptive cardiac hypertrophy and accelerates myocardial remodeling. Hypertension. 2010; 55:939–945. [PubMed: 20177000]
39. Akhmetshina A, Palumbo K, Dees C, Bergmann C, Venalis P, Zerr P, Horn A, Kireva T, Beyer C, Zwerina J, Schneider H, Sadowski A, Riener MO, MacDougald OA, Distler O, Schett G, Distler JH. Activation of canonical Wnt signalling is required for TGF-beta-mediated fibrosis. Nat Commun. 2012; 3:735. [PubMed: 22415826]

40. Kumawat K, Menzen MH, Bos IS, Baarsma HA, Borger P, Roth M, Tamm M, Halayko AJ, Simoons M, Prins A, Postma DS, Schmidt M, Noncanonical Gosens R. WNT-5A signaling regulates TGF-beta-induced extracellular matrix production by airway smooth muscle cells. FASEB J. 2013; 27:1631–1643. [PubMed: 23254341]
41. Massague J, Gomis RR. The logic of TGFbeta signaling. FEBS Lett. 2006; 580:2811–2820. [PubMed: 16678165]
42. Wrana JL, Attisano L. The Smad pathway. Cytokine Growth Factor Rev. 2000; 11:5–13. [PubMed: 10708948]
43. Lee SJ. Regulation of muscle mass by myostatin. Annu Rev Cell Dev Biol. 2004; 20:61–86. [PubMed: 15473835]
44. Ba X, Bacsi A, Luo J, Aguilera-Aguirre L, Zeng X, Radak Z, Brasier AR, Boldogh I. 8-Oxoguanine DNA glycosylase-1 augments proinflammatory gene expression by facilitating the recruitment of site-specific transcription factors. J Immunol. 2014; 192:2384–2394. [PubMed: 24489103]
45. Holmstrom KM, Finkel T. Cellular mechanisms and physiological consequences of redox-dependent signalling. Nat Rev Mol Cell Biol. 2014; 15:411–421. [PubMed: 24854789]
46. Ba X, Aguilera-Aguirre L, Rashid QT, Bacsi A, Radak Z, Sur S, Hosoki K, Hegde ML, Boldogh I. The role of 8-oxoguanine DNA glycosylase-1 in inflammation. Int J Mol Sci. 2014; 15:16975–16997. [PubMed: 25250913]
47. Ma X, Becker Buscaglia LE, Barker JR, Li Y. MicroRNAs in NF-kappaB signaling. J Mol Cell Biol. 2011; 3:159–166. [PubMed: 21502305]
48. Boldogh I, Bacsi A, Choudhury BK, Dharajiya N, Alam R, Hazra TK, Mitra S, Goldblum RM, Sur S. ROS generated by pollen NADPH oxidase provide a signal that augments antigen-induced allergic airway inflammation. J Clin Invest. 2005; 115:2169–2179. [PubMed: 16075057]
49. Bacsi A, Aguilera-Aguirre L, Szczesny B, Radak Z, Hazra TK, Sur S, Ba X, Boldogh I. Down-regulation of 8-oxoguanine DNA glycosylase 1 expression in the airway epithelium ameliorates allergic lung inflammation. DNA Repair (Amsterdam). 2013; 12:18–26.
50. Choi JH, Kim JH, Park HS. Upper airways in aspirin-exacerbated respiratory disease. Curr Opin Allergy Clin Immunol. 2015; 15:21–26. [PubMed: 25546326]
51. Jamaluddin M, Wang S, Boldogh I, Tian B, Brasier AR. TNF-alpha-induced NF-kappaB/RelA Ser(276) phosphorylation and enhanceosome formation is mediated by an ROS-dependent PKAc pathway. Cell Signalling. 2007; 19:1419–1433. [PubMed: 17317104]
52. Ijaz T, Pazdrak K, Kalita M, Konig R, Choudhary S, Tian B, Boldogh I, Brasier AR. Systems biology approaches to understanding epithelial mesenchymal transition (EMT) in mucosal remodeling and signaling in asthma. World Allergy Organ J. 2014; 7:13. [PubMed: 24982697]
53. Nowak DE, Tian B, Jamaluddin M, Boldogh I, Vergara LA, Choudhary S, Brasier AR. RelA Ser276 phosphorylation is required for activation of a subset of NF-kappaB-dependent genes by recruiting cyclin-dependent kinase 9/cyclin T1 complexes. Mol Cell Biol. 2008; 28:3623–3638. [PubMed: 18362169]
54. Weaver JR, Bartolomei MS. Chromatin regulators of genomic imprinting. Biochim Biophys Acta. 2014; 1839:169–177. [PubMed: 24345612]
55. Royce SG, Karagiannis TC. Histone deacetylases and their inhibitors: new implications for asthma and chronic respiratory conditions. Curr Opin Allergy Clin Immunol. 2014; 14:44–48. [PubMed: 24322009]
56. Strengert M, Knaus UG. Analysis of epithelial barrier integrity in polarized lung epithelial cells. Methods Mol Biol. 2011; 763:195–206. [PubMed: 21874453]
57. Hajas G, Bacsi A, Aguilerra-Aguirre L, German P, Radak Z, Sur S, Hazra TK, Boldogh I. Biochemical identification of a hydroperoxide derivative of the free 8-oxo-7,8-dihydroguanine base. Free Radic Biol Med. 2012; 52:749–756. [PubMed: 22198182]
58. Kuo PL, Hsu YL, Huang MS, Chiang SL, Ko YC. Bronchial epithelium-derived IL-8 and RANTES increased bronchial smooth muscle cell migration and proliferation by Kruppel-like factor 5 in areca nut-mediated airway remodeling. Toxicol Sci. 2011; 121:177–190. [PubMed: 21297082]

59. Takeda N, Sumi Y, Prefontaine D, Al Abri J, Al Heialy N, Al-Ramli W, Michoud MC, Martin JG, Hamid Q. Epithelium-derived chemokines induce airway smooth muscle cell migration. Clin Exp Allergy. 2009; 39:1018–1026. [PubMed: 19364333]

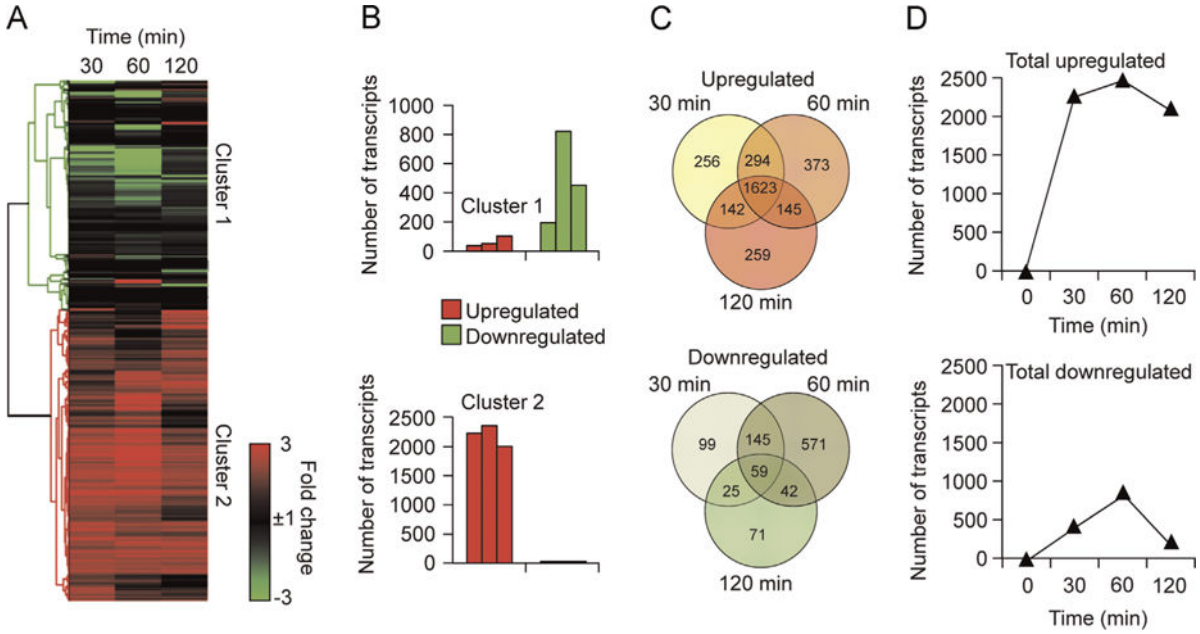


**Fig. 1.**

Whole transcriptome analysis of gene expression induced by OGG1-BER. Lungs were repeatedly challenged with the product of OGG1-BER (8-oxoG base) and total RNAs were isolated and subjected to RNA-Seq analysis as described under Materials and methods. (A) Hierarchical clustering showing changes at the whole-transcriptome level. Transcript levels (RPKM) were normalized to control (time 0 min). Heat maps were generated using GENE-E. Rows represent identified transcripts and columns the time points (30, 60, and 120 min) after 8-oxoG challenge. The intensity of the red and green colors in the heat map shows the degree of upregulation or downregulation, respectively. (B) Significantly up- and downregulated transcripts in clusters 1 and 2. The total numbers of upregulated (≥3-fold) transcripts are represented by red bars and the downregulated (≤3-fold) ones by green bars. (C) Number of unique and shared transcripts altered by 8-oxoG challenge. Venn diagrams were constructed using the Venny online software. (D) Kinetic changes in number of transcripts induced by 8-oxoG challenge as a function of time.

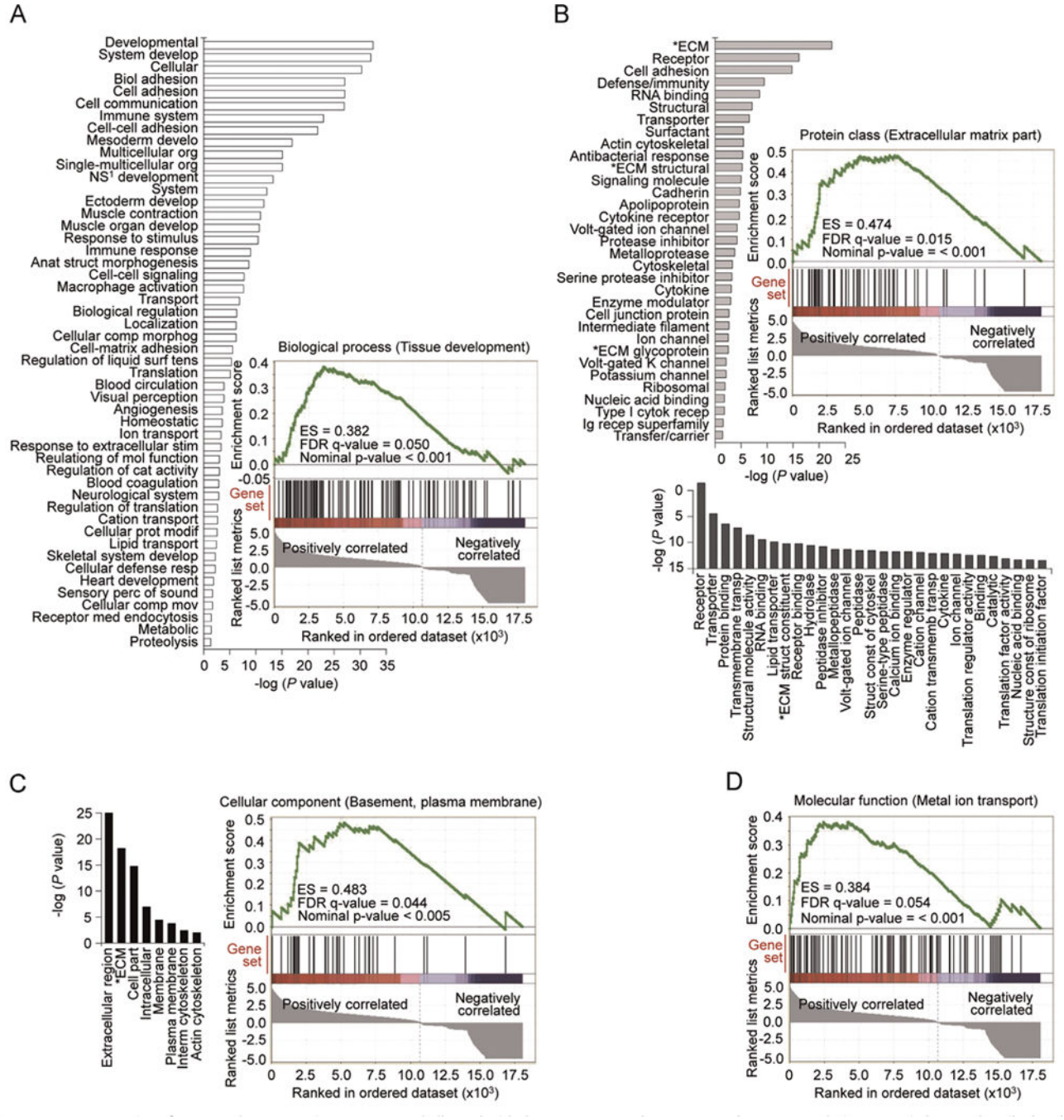


**Fig. 2.**

Overrepresentation of gene ontology categories. Lungs were challenged with the OGG1-BER product 8-oxoG and RNA-Seq analysis was carried out as described under Materials and methods. An overrepresentation test of the upregulated genes (≥ 3-fold, 60 min) was performed using PANTHER classification system (overrepresentation levels are expressed as − log(*P value*) and were confirmed by using GSEA (ES, *q*, and *p* values are included). (A) Biological process, (B) protein class, (C) cellular component, and (D) molecular function.

*ECM, extracellular matrix; Ig, immunoglobulin; NS[1], nervous system; ES, enrichment score; FDR, false discovery rate.

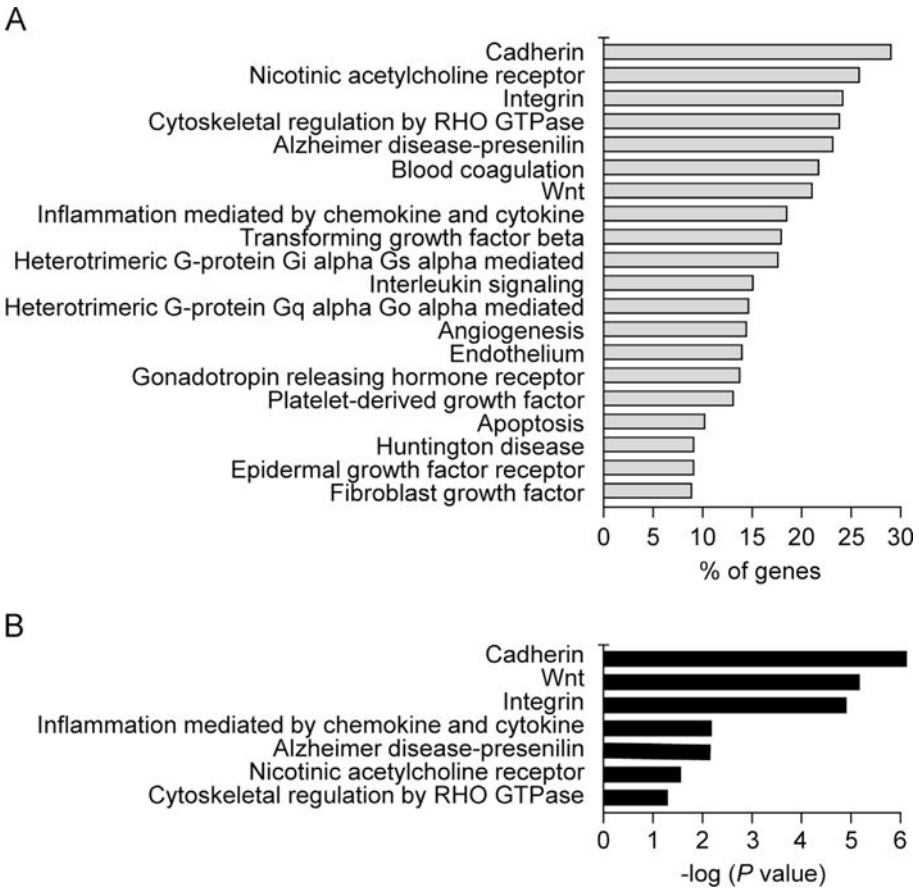


**Fig. 3.**

Signaling pathways induced by the OGG1-BER product 8-oxoG. Lungs were repeatedly challenged with 8-oxoG and RNA was analyzed (Materials and methods). PANTHER analyses were carried out using the list of upregulated genes (≥ 3-fold, 60 min) after multiple challenges with 8-oxoG. (A) Percentage of genes activated in individual signaling pathways. (B) Overrepresentation of signaling pathways. Bars represent−log(*P* value).

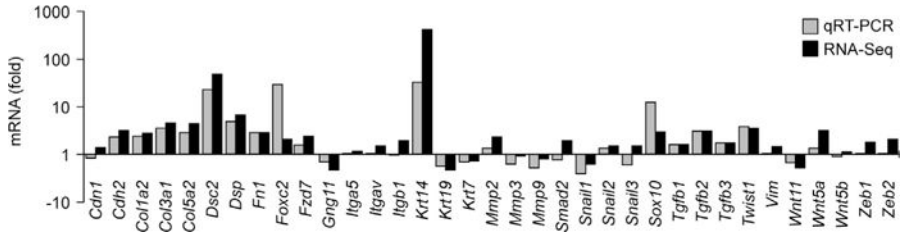


**Fig. 4.**

Validation of gene expression from RNA-Seq data by qRT-PCR. Briefly, 1 μg of pooled RNA was subjected to RNA-Seq or to reverse transcription (cDNA synthesis) for qRT-PCR analysis of selected genes related to tissue remodeling and evaluated by the $\Delta\Delta C_t$ method as described under Materials and methods. Black bars, RNA-Seq; gray bars, qRT-PCR.

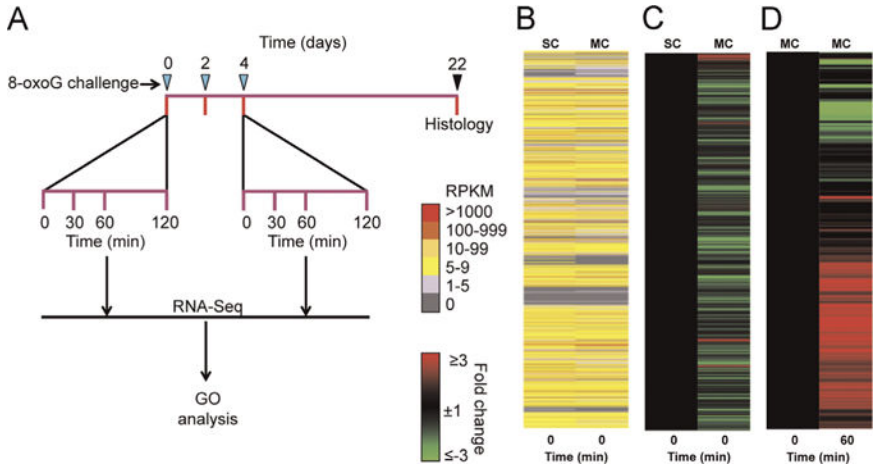


**Fig. 5.**

Tissue remodeling-associated gene expression induced by multiple challenges. (A) Experimental design: mice were challenged i.n. with the OGG1-BER product 8-oxoG at days 0, 2, and 4. On days 0 and 4, RNA was isolated after 0, 30, 60, and 120 min for whole transcriptome analysis by RNA-Seq and gene ontology. (B) Differences in RPKM levels between SC and MC at time 0. (C) Fold changes in transcript levels after MC compared to SC at time 0. (D) Fold changes in transcript levels induced by multiple challenges at 60 min compared to time 0. Expression values at 0 min were taken as onefold (D, left).

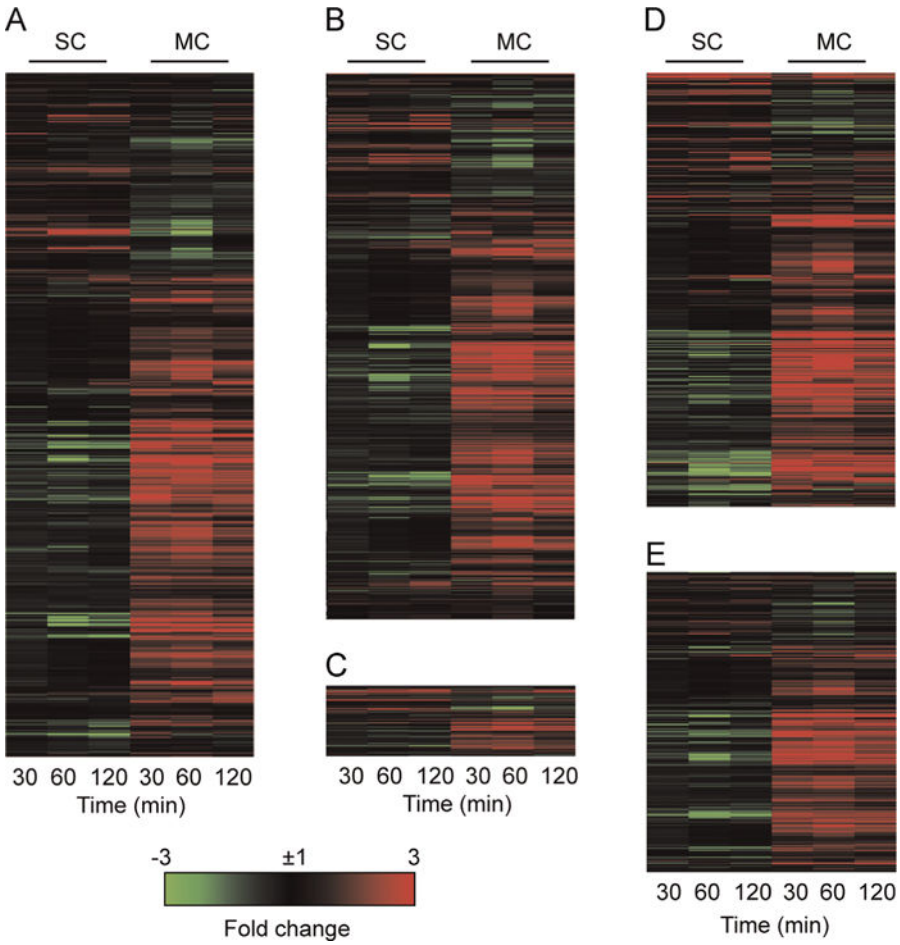


**Fig. 6.**

Relevance of 8-oxoG-induced gene expression to human tissue eremodeling. Gene lists were generated based on the Gene Cards database and searched against our RNA-Seq datasets to visualize expression patterns of genes linked to human tissue remodeling. (A) Cytoskeleton, (B) cell adhesion, (C) surfactant, (D) extracellular matrix, and (E) cell junction. SC, single challenge; MC, multiple challenges.

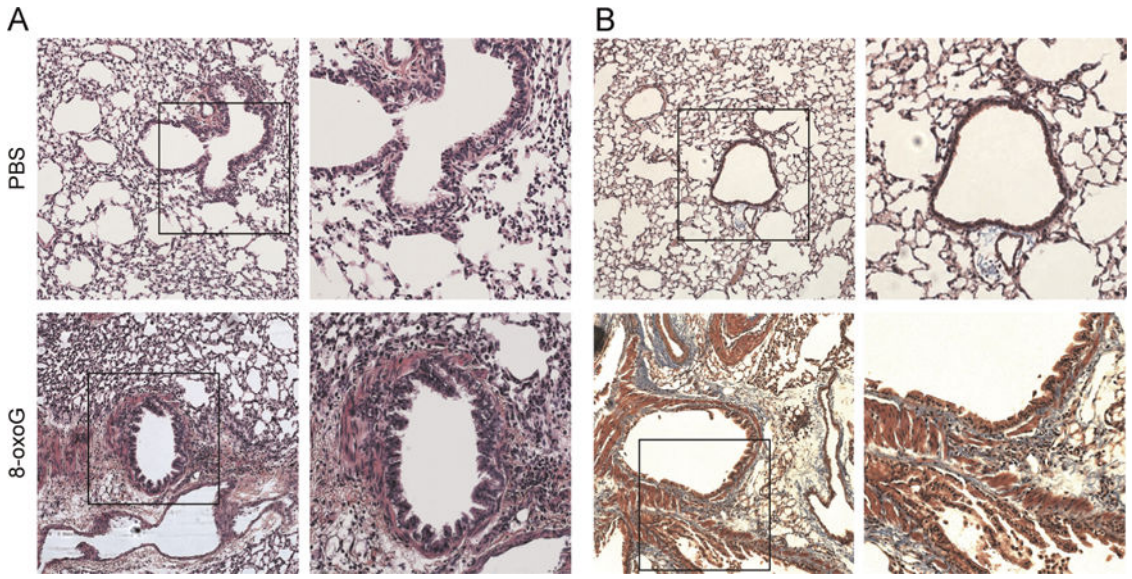


**Fig. 7.**

Histological changes in mouse airways after challenge with 8-oxoG released from DNA by OGG1-BER. Mice were challenged with 8-oxoG on days 0, 2, and 4. On day 22, lungs were sectioned, stained, and examined microscopically. (A) Hematoxylin and eosin staining of vehicle-treated (top) and 8-oxoG-challenged (bottom) lungs. (B) Masson's trichrome-stained lung sections showing collagen deposition (blue, bottom). Original magnifications in (A) and (B) were 96 × (left) and 192 × (right).

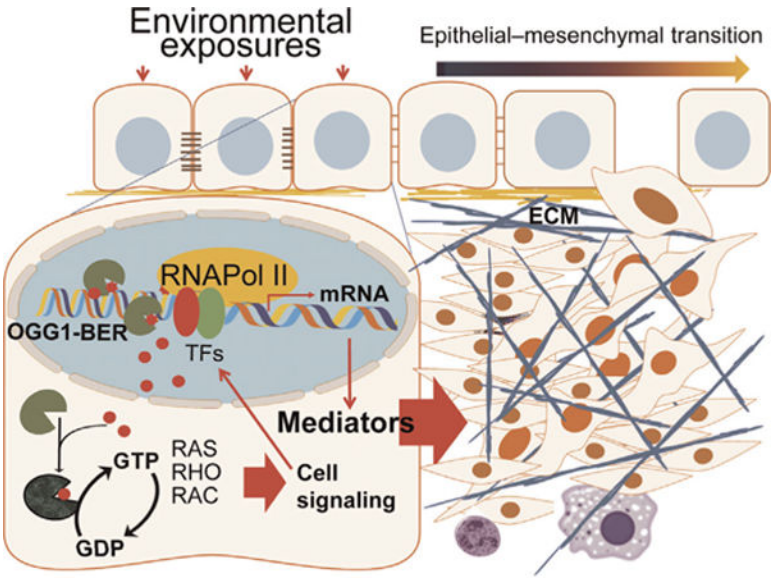


**Fig. 8.**

A proposed model for OGG1-BER-driven tissue remodeling. The repair product of OGG1-BER, 8-oxoG base, is bound by cytosolic OGG1 and the complex increases the levels of activated (GTP-bound) small GTPases. Downstream signaling activates transcription factors (TFs) and the expression of mediators, responsible for changes in both the mucosal epithelium (e.g., epithelial–mesenchymal transition) and the subepithelial tissues (e.g., smooth muscle proliferation and increased ECM).

## Table 1

OGG1-BER-induced genes related to signaling pathways involved in airway remodeling

| Symbol | Name | GenBank/Ref-Seq ID | Fold |
|---|---|---|---|
| Cadherinsignaling pathway | | | |
| *Acta1* | Actin, α1, skeletal muscle | NM_009606 | 478.01 |
| *Actc1* | Actin, α, cardiac muscle 1 | NM_009608 | 3.93 |
| *Cdh13* | Cadherin 13 | NM_019707 | 18.33 |
| *Cdh15* | Cadherin 15 | NM_007662 | 3.92 |
| *Cdh19* | Cadherin 19, type 2 | NM_001081386 | 36.86 |
| *Cdh2* | Cadherin 2 | NM_007664 | 3.21 |
| *Cdh3* | Cadherin 3 | NM_007665 | 14.56 |
| *Cdh6* | Cadherin 6 | NM_007666 | 9.01 |
| *Cdh8* | Cadherin 8 | NM_007667 | 3.35 |
| *Ctnna2* | Catenin (cadherin-associated protein), α2 | NM_009819 | 14.24 |
| *Ctnna3* | Catenin (cadherin-associated protein), α3 | NM_177612 | 4.11 |
| *Egfr* | Epidermal growth factor receptor | NM_007912 | 3.05 |
| *Erbb3* | V-erb-b2 erythroblastic leukemiaviral oncogene homolog 3 (avian) | NM_010153 | 42.81 |
| *Erbb4* | V-erb-a erythroblastic leukemiaviral oncogene homolog 4 (avian) | NM_010154 | 7.96 |
| *Fat3* | FAT tumor suppressor homolog 3(*Drosophila*) | NM_001080814 | 3.18 |
| *Fzd10* | Frizzled homolog 10 (*Drosophila*) | NM_175284 | 12.37 |
| *Fzd4* | Frizzled homolog 4 (*Drosophila*) | NM_008055 | 7.29 |
| *Fzd9* | Frizzled homolog 9 (*Drosophila*) | NM_010246 | 3.15 |
| *Lef1* | Lymphoid enhancer binding factor 1 | NM_010703 | 6.38 |
| *Pcdh15* | Protocadherin 15 | NM_023115 | 20.74 |
| *Pcdh20* | Protocadherin 20 | NM_178685 | 6.18 |
| *Pcdh7* | Protocadherin 7 | NM_001122758 | 4.87 |
| *Pcdh9* | Protocadherin 9 | NM_001271800 | 6.28 |
| *Pcdhb10* | Protocadherin β10 | NM_053135 | 3.25 |
| *Pcdhb11* | Protocadherin β11 | NM_053136 | 5.36 |
| *Pcdhb12* | Protocadherin β12 | NM_053137 | 3.10 |
| *Pcdhb13* | Protocadherin β13 | NM_053138 | 4.10 |
| *Pcdhb2* | Protocadherin β2 | NM_053127 | 7.06 |
| *Pcdhb21* | Protocadherin β21 | NM_053146 | 9.22 |
| *Pcdhb4* | Protocadherin β4 | NM_053129 | 3.42 |
| *Pcdhb8* | Protocadherin β8 | NM_053133 | 87.55 |
| *Wnt10a* | Wingless-type MMTV integration site family, member 10A | NM_009518 | 7.90 |
| *Wnt2b* | Wingless-type MMTV integration site family, member 2B | NM_009520 | 4.97 |
| *Wnt4* | Wingless-type MMTV integration site family, member 4 | NM_009523 | 3.46 |
| *Wnt5a* | Wingless-type MMTV integration site family, member 5A | NM_009524 | 3.18 |
| *Wnt7b* | Wingless-type MMTV integration site family, member 7B | NM_009528 | 3.20 |
| *Wnt9b* | Wingless-type MMTV integration site family, member 9B | NM_011719 | 7.54 |
| Integrinsignaling pathway | | | |

| Symbol | Name | GenBank/Ref-Seq ID | Fold |
|---|---|---|---|
| *Abl1* | C-abl oncogene 1, nonreceptor tyrosine kinase | NM_009594 | 3.01 |
| *Actn2* | Actinin α2 | NM_033268 | 10.19 |
| *Actn3* | Actinin α3 | NM_013456 | 305.45 |
| *Arl1* | ADP-ribosylation factor-like 1 | NM_025859 | 4.83 |
| *Asap1* | ArfGAP with SH3 domain, ankyrinrepeat, and PH domain 1 | NM_010026 | 3.53 |
| *Col10a1* | Collagen, type X, α1 | NM_009925 | 21.19 |
| *Col11a1* | Collagen, type XI, α1 | NM_007729 | 7.86 |
| *Col11a2* | Collagen, type XI, α2 | NM_009926 | 3.17 |
| *Col13a1* | Collagen, typeXIII, α1 | NM_007731 | 3.14 |
| *Col14a1* | Collagen, type XIV, α1 | NM_181277 | 4.03 |
| *Col15a1* | Collagen, type XV, α1 | NM_009928 | 4.38 |
| *Col17a1* | Collagen, type XVII, α1 | NM_007732 | 6.73 |
| *Col1a1* | Collagen, type I, α1 | NM_007742 | 5.03 |
| *Col2a1* | Collagen, type II, α1 | NM_031163 | 5.73 |
| *Col3a1* | Collagen, type III, α1 | NM_009930 | 4.71 |
| *Col4a* | Collagen, type IV, α1 | NM_009931 | 3.95 |
| *Col4a2* | Collagen, type IV, α2 | NM_009932 | 3.61 |
| *Col4a3* | Collagen, type IV, α3 | NM_007734 | 6.74 |
| *Col4a4* | Collagen, type IV, α4 | NM_007735 | 5.51 |
| *Col5a1* | Collagen, type V, α1 | NM_015734 | 3.64 |
| *Col5a2* | Collagen, type V, α2 | NM_007737 | 4.45 |
| *Col5a3* | Collagen, type V, α3 | NM_016919 | 4.35 |
| *Col6a3* | Collagen, type VI, α3 | NM_009935 | 3.24 |
| *Col6a6* | Collagen, type VI, α6 | NM_172927 | 28.37 |
| *Col8a1* | Collagen, type VIII, α1 | NM_007739 | 4.93 |
| *Col9a1* | Collagen, type IX, α1 | NM_007740 | 8.62 |
| *Col9a2* | Collagen, type IX, α2 | NM_007741 | 4.51 |
| *Crkl* | V-crk sarcoma virus CT10 oncogene homolog (avian)-like | NM_007764 | 14.51 |
| *Itga1* | Integrin α1 | NM_001033228 | 3.68 |
| *Itga2* | Integrin α2 | NM_008396 | 16.01 |
| Itga6 | Integrin α6 | NM_008397 | 29.12 |
| *Itgad* | Integrin αD | NM_001029872 | 4.72 |
| *Itgam* | Integrin αM | NM_008401 | 3.66 |
| *Itgbl1* | Integrin, *β*-like 1 | NM_145467 | 3.47 |
| *Lama2* | Laminin α2 | NM_008481 | 4.08 |
| *Lama3* | Laminin α3 | NM_010680 | 3.94 |
| *Lamb1* | Laminin B1 | NM_008482 | 3.01 |
| *Lamc1* | Laminin γ1 | NM_010683 | 4.35 |
| *Mapk6* | Mitogen-activated protein kinase 6 | NM_015806 | 3.08 |
| *Megf9* | Multiple EGF-like-domains 9 | NM_172694 | 18.10 |
| *Ntn4* | Netrin 4 | NM_021320 | 18.49 |
| *Pik3r1* | Phosphatidylinositol 3-kinase, regulatory subunit, polypeptide 1 | NM_001077495 | 3.24 |

| Symbol | Name | GenBank/Ref-Seq ID | Fold |
|---|---|---|---|
| Rho GTPase signaling pathway | | | |
| *Acta1* | Actin, α1, skeletal muscle | NM_009606 | 478.01 |
| *Actc1* | Actin, α, cardiac muscle 1 | NM_009608 | 3.93 |
| *Diap1* | Diaphanous homolog 1 (*Drosophila*) | NM_007858 | 9.85 |
| *Diap2* | Diaphanous homolog 2 (*Drosophila*) | NM_017398 | 3.18 |
| *Diap3* | Diaphanous homolog f3(*Drosophila*) | NM_019670 | 15.39 |
| *Myh1* | Myosin, heavy polypeptide 1, skeletal muscle, adult | NM_030679 | 1133.76 |
| *Myh10* | Myosin, heavy polypeptide 10,nonmuscle | NM_175260 | 3.08 |
| *Myh11* | Myosin, heavy polypeptide 11,smooth muscle | NM_013607 | 5.09 |
| *Myh13* | Myosin, heavy polypeptide 13, skeletal muscle | NM_001081250 | 14.31 |
| *Myh2* | Myosin, heavy polypeptide 2, skeletal muscle, adult | NM_144961 | 809.14 |
| *Myh3* | Myosin, heavy polypeptide 3, skeletal muscle, embryonic | NM_001099635 | 43.64 |
| *Myh4* | Myosin, heavy polypeptide 4, skeletal muscle | NM_010855 | 656.96 |
| *Myh8* | Myosin, heavy polypeptide 8, skeletal muscle, perinatal | NM_177369 | 1360.71 |
| *Myh9* | Myosin, heavy polypeptide 9,nonmuscle | NM_022410 | 3.25 |
| *Mylk2* | Myosin, light polypeptide kinase 2,skeletal muscle | NM_001081044 | 97.19 |
| *Pak3* | P21 protein (Cdc42/Rac)-activated kinase 3 | NM_008778 | 5.49 |
| *Ssh1* | Slingshot homolog 1 (*Drosophila*) | NM_198109 | 8.69 |
| *Tubb1* | Tubulin, β1 class VI | NM_001080971 | 18.37 |
| Wnt signaling pathway | | | |
| *Acta1* | Actin, α1, skeletal muscle | NM_009606 | 478.01 |
| *Actc1* | Actin, α, cardiac muscle 1 | NM_009608 | 3.93 |
| *Bcl9* | B cell CLL/lymphoma 9 | NM_029933 | 8.59 |
| *Cdh2* | Cadherin 2 | NM_007664 | 3.21 |
| *Cdh3* | Cadherin 3 | NM_007665 | 14.56 |
| *Cdh6* | Cadherin 6 | NM_007666 | 9.01 |
| *Cdh8* | Cadherin 8 | NM_007667 | 3.35 |
| *Cdh13* | Cadherin 13 | NM_019707 | 18.33 |
| *Cdh15* | Cadherin 15 | NM_007662 | 3.92 |
| *Cdh19* | Cadherin 19, type 2 | NM_001081386 | 36.86 |
| *Crebbp* | CREB binding protein | NM_001025432 | 9.85 |
| *Ctnna2* | Catenin (cadherin-associated protein), α2 | NM_009819 | 14.24 |
| *Ctnna3* | Catenin (cadherin-associated protein), α3 | NM_177612 | 4.11 |
| *Dvl3* | Dishevelled 3, dsh homolog (*Drosophila*) | NM_007889 | 8.95 |
| *Edn1* | Endothelin 1 | NM_010104 | 3.81 |
| *Fat3* | FAT tumor suppressor homolog 3 (*Drosophila*) | NM_001080814 | 3.18 |
| *Frzb* | Frizzled-related protein | NM_011356 | 11.53 |
| *Fzd4* | Frizzled homolog 4 (*Drosophila*) | NM_008055 | 7.29 |
| *Fzd9* | Frizzled homolog 9 (*Drosophila*) | NM_010246 | 3.15 |
| *Fzd10* | Frizzled homolog 10 (*Drosophila*) | NM_175284 | 12.37 |
| *Gng3* | Guanine nucleotide binding protein(G protein), γ3 | NM_010316 | 3.05 |
| *Itpr2* | Inositol 1,4,5-triphosphate receptor 2 | NM_010586 | 3.39 |

| Symbol | Name | GenBank/Ref-Seq ID | Fold |
|---|---|---|---|
| *Lef1* | Lymphoid enhancer binding factor 1 | NM_010703 | 6.38 |
| *Lrp5* | Low-density lipoprotein receptor-related protein 5 | NM_008513 | 4.22 |
| *Myh1* | Myosin, heavy polypeptide 1, skeletal muscle, adult | NM_030679 | 1133.76 |
| *Myh2* | Myosin, heavy polypeptide 2, skeletal muscle, adult | NM_144961 | 809.14 |
| *Myh3* | Myosin, heavy polypeptide 3, skeletal muscle, embryonic | NM_001099635 | 43.64 |
| *Myh4* | Myosin, heavy polypeptide 4, skeletal muscle | NM_010855 | 656.96 |
| *Myh8* | Myosin, heavy polypeptide 8, skeletal muscle, perinatal | NM_177369 | 1360.71 |
| *Myh13* | Myosin, heavy polypeptide 13, skeletal muscle | NM_001081250 | 14.31 |
| *Nfatc2* | NF$^a$ of activated T cells, cytoplasmic, calcineurin-dependent 2 | NM_010899 | 3.43 |
| *Nkd2* | Naked cuticle 2 homolog (*Drosophila*) | NM_028186 | 3.32 |
| *Pcdh7* | Protocadherin 7 | NM_001122758 | 4.87 |
| *Pcdh9* | Protocadherin 9 | NM_001271800 | 6.28 |
| *Pcdh15* | Protocadherin 15 | NM_023115 | 20.74 |
| *Pcdh20* | Protocadherin 20 | NM_178685 | 6.18 |
| *Pcdhb2* | Protocadherin β2 | NM_053127 | 7.06 |
| *Pcdhb4* | Protocadherin β4 | NM_053129 | 3.42 |
| *Pcdhb8* | Protocadherin β8 | NM_053133 | 87.55 |
| *Pcdhb10* | Protocadherin β10 | NM_053135 | 3.25 |
| *Pcdhb11* | Protocadherin β11 | NM_053136 | 5.36 |
| *Pcdhb12* | Protocadherin β12 | NM_053137 | 3.10 |
| *Pcdhb13* | Protocadherin β13 | NM_053138 | 4.10 |
| *Pcdhb21* | Protocadherin β21 | NM_053146 | 9.22 |
| *Plcb4* | Phospholipase C, β4 | NM_013829 | 26.96 |
| *Sfrp1* | Secreted frizzled-related protein 1 | NM_013834 | 3.32 |
| *Sfrp2* | Secreted frizzled-related protein 2 | NM_009144 | 15.17 |
| *Sfrp4* | Secreted frizzled-related protein 4 | NM_016687 | 3.75 |
| *Tbl1x* | Transducin (β)-like 1 X-linked | NM_020601 | 9.74 |
| *Tcf7* | Transcription factor 7, T-cell-specific | NM_009331 | 4.31 |
| *Tnf* | Tumor necrosis factor | NM_013693 | 7.13 |
| *Wnt10a* | Wingless-type MMTV integration site family, member 10A | NM_009518 | 7.90 |
| *Wnt2b* | Wingless-type MMTV integration site family, member 2B | NM_009520 | 4.97 |
| *Wnt4* | Wingless-type MMTV integration site family, member 4 | NM_009523 | 3.46 |
| *Wnt5a* | Wingless-type MMTV integration site family, member 5A | NM_009524 | 3.17 |
| *Wnt7b* | Wingless-type MMTV integration site family, member 7B | NM_009528 | 3.20 |
| *Wnt9b* | Wingless-type MMTV integration site family, member 9B | NM_011719 | 7.54 |
| *TGF-β s*ignaling pathway | | | |
| *Acvr1b* | Activin A receptor, type 1B | NM_007395 | 7.02 |
| *Acvr1c* | Activin A receptor, type 1C | NM_001111030 | 8.30 |
| *Bmp5* | Bone morphogenetic protein 5 | NM_007555 | 8.48 |
| *Bmp6* | Bone morphogenetic protein 6 | NM_007556 | 6.85 |
| *Bmp8a* | Bone morphogenetic protein 8a | NM_007558 | 4.82 |
| *Bmpr2* | Bone morphogenetic protein receptor, type II | NM_007561 | 6.75 |

| Symbol | Name | GenBank/Ref-Seq ID | Fold |
|---|---|---|---|
| *Cited4* | Cbp/p300-interacting transactivator, terminal d4 | NM_019563 | 3.22 |
| *Crebbp* | CREB binding protein | NM_001025432 | 9.85 |
| *Fosl1* | Fos-like antigen 1 | NM_010235 | 7.52 |
| *Foxh1* | Forkhead box H1 | NM_007989 | 3.35 |
| *Gdf2* | Growth differentiation factor 2 | NM_019506 | 12.15 |
| *Gdf6* | Growth differentiation factor 6 | NM_013526 | 7.54 |
| *Gdf11* | Growth differentiation factor 11 | NM_010272 | 5.15 |
| *Mstn* | Myostatin | NM_010834 | 48.87 |
| *Tgfb2* | Transforming growth factor, β2 | NM_009367 | 3.12 |
| *Tll1* | Tolloid-like | NM_009390 | 5.98 |
| *Zfyve9* | Zinc finger, FYVE domain containing 9 | NM_183300 | 6.90 |
| *Cytokine* and chemokine signaling pathway | | | |
| *Adcy5* | Adenylate cyclase 5 | NM_001012765 | 3.68 |
| *Alox12* | Arachidonate 12-lipoxygenase | NM_007440 | 3.07 |
| *Alox12e* | Arachidonate lipoxygenase, epidermal | NM_145684 | 3.83 |
| *Camk2a* | Calcium/calmodulin-dependentprotein kinase IIα | NM_009792 | 6.08 |
| *Ccl3* | Chemokine (C-C motif) ligand 3 | NM_011337 | 9.19 |
| *Ccr4* | Chemokine (C-C motif) receptor 4 | NM_009916 | 5.07 |
| *Ccr6* | Chemokine (C-C motif) receptor 6 | NM_009835 | 22.48 |
| *Ccr8* | Chemokine (C-C motif) receptor 8 | NM_007720 | 11.87 |
| *Ccr9* | Chemokine (C-C motif) receptor 9 | NM_009913 | 6.19 |
| *Ccl20* | Chemokine (C-C motif) ligand 20 | NM_016960 | 7.64 |
| *Col6a3* | Collagen, type VI, α3 | NM_009935 | 3.24 |
| *Col6a6* | Collagen, type VI, α6 | NM_172927 | 28.37 |
| *Col14a1* | Collagen, type VI, α3 | NM_009935 | 4.03 |
| *Cxcl1* | Chemokine (C-X-C motif) ligand 1 | NM_008176 | 15.94 |
| *Cxcl2* | Chemokine (C-X-C motif) ligand 2 | NM_009140 | 48.55 |
| *Cxcl3* | Chemokine (C-X-C motif) ligand 3 | NM_203320 | 12.33 |
| *Cxcl9* | Chemokine (C-X-C motif) ligand 9 | NM_008599 | 9.09 |
| *Cxcl10* | Collagen, type VI, α6 | NM_172927 | 13.57 |
| *Cxcl11* | Chemokine (C-X-C motif) ligand 11 | NM_019494 | 16.02 |
| *Cxcl12* | Chemokine (C-X-C motif) ligand 12 | NM_021704 | 3.44 |
| *Cxcl13* | Chemokine (C-X-C motif) ligand 13 | NM_018866 | 8.05 |
| *Gng3* | Collagen, type XIV, α1 | NM_181277 | 3.05 |
| *Grap2* | Chemokine (C-X-C motif) ligand 10 | NM_021274 | 3.53 |
| *Il1a* | Interleukin 1α | NM_010554 | 5.55 |
| *Il2rb* | Interleukin 2 receptor, β chain | NM_008368 | 4.04 |
| *Il10* | Interleukin 10 | NM_010548 | 33.51 |
| *Il17c* | Interleukin 17C | NM_145834 | 5.24 |
| *Itga2* | Integrin α2 | NM_008396 | 16.01 |
| *Itgam* | Integrin αM | NM_008401 | 3.66 |
| *Itpr2* | Inositol 1,4,5-triphosphate receptor | NM_010586 | 3.39 |

| Symbol | Name | GenBank/Ref-Seq ID | Fold |
|---|---|---|---|
| *Nfatc2* | NF[a] of activated T cells, calcineurin-dependent 2 | NM_010899 | 3.43 |
| *Nfkbia* | NF[a] of κ LP[b] gene enhancer in B cells inhibitor, α | NM_010907 | 4.41 |
| *Pak3* | P21 protein (Cdc42/Rac)-activated kinase 3 | NM_008778 | 5.49 |
| *Plcb4* | Phospholipase C, β4 | NM_013829 | 26.96 |
| *Plcg1* | Phospholipase C, γ1 | NM_021280 | 17.11 |
| *Prkx* | Protein kinase, X-linked | NM_016979 | 14.88 |
| *Ptafr* | Platelet-activating factor receptor | NM_001081211 | 4.56 |
| *Rel* | Reticuloendotheliosis oncogene | NM_009044 | 4.27 |
| *Rgs1* | Regulator of G-protein signaling 1 | NM_015811 | 5.85 |
| *Socs4* | Suppressor of cytokine signaling 4 | NM_080843 | 4.35 |
| *Vwa2* | Von Willebrand factor A domain-containing 2 | NM_172840 | 3.26 |

[a]Nuclear factor.

[b]Long peptide.